Macromolecules
ARTICLE

Macromolecules **2010**, *43*, 5137–5148 **5137**
DOI: 10.1021/ma100414u

Interplay between Chain Collapse and Microphase Separation in Bottle-Brush Polymers with Two Types of Side Chains

Panagiotis E. Theodorakis,*[,†] Wolfgang Paul,[†,‡] and Kurt Binder[†]

[†]*Institut für Physik, Johannes Gutenberg-Universität, Mainz, Staudinger Weg 7, D-55099 Mainz, Germany, and* [‡]*Martin-Luther-Universität Halle-Wittenberg, Institut für Physik, von-Seckendorff-Platz 1, 06120 Halle, Germany*

Received February 23, 2010

ABSTRACT: Conformations of a bottle-brush polymer with two types (A,B) of grafted side chains are studied by molecular dynamics simulations, using a coarse-grained bead−spring model with side chains of up to $N = 50$ effective monomers. Varying the solvent quality and the grafting density, the crossover from the "pearl-necklace" structure to dense cylinders is studied. Whereas for small grafting density, A- and B-chains form separate collapsed chains, at intermediate grafting density, larger "pearls" containing several chains are observed, exhibiting microphase separation between A and B in "dumbbell"-type configurations. At still larger grafting density, short-range order of "Janus dumbbell"-type is observed. It is argued that because of the quasi-1D character of bottle-brush polymers with stiff backbones, all phase changes occur gradually, and no sharp-phase transitions like in bulk polymer mixtures or block copolymer melts can be observed.

I. Introduction

Recently there has been a lot of interest in macromolecules with bottle-brush architecture,[1−21] where (flexible) side chains are grafted on a backbone chain molecule that may either be intrinsically rigid already, or, when it is intrinsically flexible, gets stiffened as a result of the excluded volume interactions between the side chains. These molecules are considered in the context of various applications (building blocks in supramolecular structures, sensors, actuators, etc.[6,7]) because these stimuli-responsive polymers may show large conformational changes when external conditions (e.g., solvent quality) are varied. Also, in a biological context, sometimes bottle-brush polymers are found, for example, aggrecane molecules are found in the soft layers in mammalian joints and held partially responsible for the excellent lubrication properties of these layers.[17] Similar structures are also found in neurofilaments.[21]

Of course, tailoring the properties of such macromolecules with rather complex architecture in view of such possible functions requires a very good understanding of structure−property relationships. However, clarifying the structure of bottle-brush polymers is already very difficult even for the simplest case, where only a single type of side chains occurs and good solvent conditions are used, because of the multitude of length scales characterizing the structure.[9−12,18] Computer simulations have proven to be very useful to validate approximations needed to interpret experimental data.[15−28] Because some of the suggested applications require to consider bottle-brush polymers under poor solvent conditions, first steps to consider this case by theory[29] and simulations have been taken as well.[30,31] For bottle-brush polymers with a single type of side chains, interesting "pearl-necklace"-type structures have been theoretically predicted[29] and observed by simulations.[31] Here we extend this work to consider bottle-brush polymers with two types of side chains; varying both grafting density and solvent quality, we focus on the interplay of density and composition variations in the direction along the backbone of the cylindrical brush. Previous work[26,32−34] has almost exclusively considered only microphase separation of "Janus cylinder"-type, whereas we show here that a much richer scenario of possible microphase-separated structures exists.

In the next section, we give a brief summary of the theoretical background, whereas in Section III, we present the model that is simulated and define the quantities that are analyzed. Section IV discusses our numerical results, whereas Section V presents our conclusions.

II. Theoretical Background

Microphase separation in one-component polymer brushes under poor solvent conditions and in two-component polymer brushes (where one can consider this phenomenon also for good solvent and theta solvent conditions) has first been studied for chains grafted onto planar substrates.[35−46] Whereas the collapse transition of a single-component polymer brush for finite chain length, N, is widely believed to occur gradually,[47−49] although this view recently has been challenged,[50] microphase separation in 2D geometry clearly is a well-defined sharp phase transition (if one disregards possible rounding of the transition caused by the quenched randomness of the fluctuations in the grafting density of the chains, which may act like a random field in the 2D Ising model[51−53]). Similarly, the microphase separation in two-component polymer brushes[42−45] involves well-defined phase transitions, analogous to order−disorder transitions in block copolymer melts,[54,55] but in this case, again the quenched random disorder in the grafting sites destroys the mesophase long-range order.[46]

Grafting side chains on a straight line, modeling bottle-brush polymers with fairly rigid backbones, leads to quasi-1D analogs of these microphase separation phenomena. In 1D systems with short-range interactions, however, statistical thermal fluctuations destroy long-range order, as is rather generally known.[56,57] Therefore, also for a binary bottle-brush polymer, one does not expect long-range order of Janus cylinder-type but rather expects such an order only to persist over a finite correlation length

*Corresponding author.

Published on Web 05/04/2010

(which, however, can be rather long when the side chain length is long).[34]

In real systems, the thermal fluctuations compete with quenched random fluctuations in the density of grafting sites along the backbone, and it is a subtle issue which of these fluctuations is more relevant for limiting the extent of local microphase separation ordering. The study of this issue is beyond the scope of the present work, however. Because as a result of such effects, no really sharp phase transitions are expected, we shall not describe any detailed calculations to derive phase boundaries here but only give qualitative arguments to understand the phenomena observed in our simulations (Section III).

We first consider the case of one-component bottle-brush polymers, following the treatment of Sheiko et al.[29] using simple scaling arguments[58] to discuss the (cross-sectional) linear dimension of a side chain of length, N, in the directions perpendicular to the backbone (which we assume to be oriented along the z axis). Under good solvent conditions, we simply have[26,59−66]

$$R_{cs} = N^{\nu} f(N^{\nu}\sigma) \rightarrow \sigma^{(1-\nu)/(1+\nu)} N^{2\nu/(1+\nu)}, \quad N \rightarrow \infty \qquad (1)$$

where $\nu \approx 0.588$ is the exponent characterizing the radius of a polymer chain under good solvent conditions,[57,67] σ is the grafting density, and f is a scaling function, which describes the crossover from individual polymer "mushrooms"[68] grafted to the backbone to the bottle-brush, where the densely grafted side chains are strongly stretched out in radial direction. Because for polymer mushrooms the linear dimension R_z in axial direction also scales as $R_z \propto N^{\nu}$, the argument $N^{\nu}\sigma$ simply tells that neighboring grafting chains along the axis start to interact when the distance between their grafting sites, σ^{-1}, becomes comparable to the dimension R_z: then, excluded volume interactions among the monomers of neighboring "mushrooms" start to cause chain stretching in radial direction, so neighboring grafting chains start to avoid each other.

Note that the power law $R_{cs} \propto N^{2\nu/(1+\nu)}$ can only be reached for very long chains, for which there also is a significant regime where the radial monomer density profile decays with a related power law[26,59−65]

$$\rho(r) \propto [r/\sigma]^{-(3\nu-1)/2\nu} \approx [r/\sigma]^{-0.65}, \quad a \ll r \leq R_{cs} \qquad (2)$$

a being the distance between (effective) monomers along a side chain. As discussed in ref 26, for most cases of practical interest, one does not reach the regime where eqs 1 and 2 hold, and henceforth we shall not discuss this good solvent regime further.

Equation 1 nevertheless inspires the treatment of the side chain linear dimensions under theta solvent conditions and also for temperatures, T, less than the theta temperature. As is well known, chain radii at $T = \Theta$ behave as $R \propto N^{1/2}$,[58] and hence

$$R_{cs} = N^{1/2} f(N^{1/2}\sigma) \qquad (3)$$

Again, neighboring chains start to interact if their distance σ^{-1} equals their unperturbed size ($\propto N^{1/2}$). The treatment based on the self-consistent field theory[61] shows that for long chains, the chains are still stretched in radial direction

$$R_{cs} \propto \sigma^{1/3} N^{2/3}, \quad f(X \gg 1) \propto X^{1/3} \qquad (4)$$

Note that eq 2 then still holds but with $\nu = 1/2$, and hence $\rho(r) \propto (r/\sigma)^{-1/2}$. When one considers the collapse of a single chain in solution when the temperature is lowered from $T > \Theta$ to $T < \Theta$, there is another crossover scaling law

$$R = N^{1/2} F(N^{1/2}\tau), \quad \tau = 1 - T/\Theta \qquad (5)$$

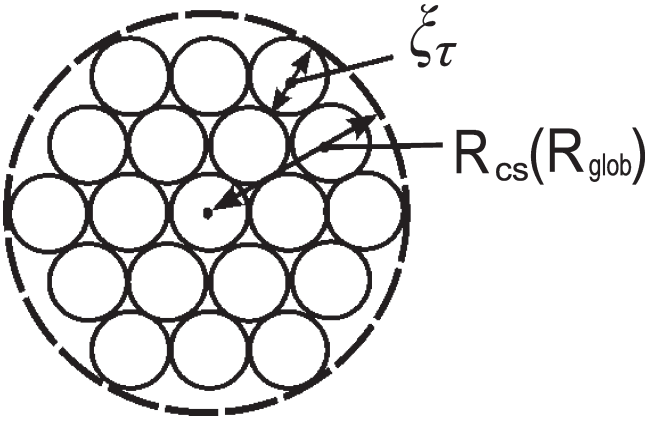

Figure 1. Blob picture of a collapsed globule of radius, R_{glob}, or of the cross-section of a collapsed cylindrical bottle-brush polymer of cross-sectional radius, R_{cs}. In both cases, thermal blobs of diameter $\xi_T \propto a/(1-T/\Theta)$ are densely packed up to the radius R_{glob} of the globule (or up to the radius R_{cs} of the cylinder, respectively). Inside the blobs, the chain conformations are Gaussian.

Here τ^{-1} is proportional to the size of "thermal blobs".[58] Note that $F(X \gg 1) \propto X^{-1/3}$, and hence for $T < \Theta$, one finds compact globules, $R \propto N^{1/3}$. Inside of a thermal blob, the chain configuration still is ideal, and hence we have $\xi_T^2 = a^2 n$, where a is the size of a monomer and we have n monomers per blob. The total number of blobs is $n_B = N/n = a^2 N/\xi_T^2$. One blob takes a volume of order ξ_T^3 (disregarding geometric factors of order unity throughout). For $T < \Theta$, the state of the chain can be interpreted as a dense packing of blobs (Figure 1), and so the radius of the globule is found from putting

$$R_{glob}^3 = n_b \xi_T^3 \Rightarrow R_{glob}/a \propto N^{1/3} (\xi_T/a)^{-1/3} \qquad (6)$$

A basic statement of the description of collapsed globules below the theta temperature hence is that inside of such globules the monomer density is essentially constant, namely, of the order

$$\rho = n/\xi_T^3 = 1/(a^2 \xi_T) \propto (1 - T/\Theta) \qquad (7)$$

When one now extends the treatment to consider bottle-brush polymers under poor solvent conditions, the scaling descriptions, eqs 3−5, need to be combined[29]

$$R_{cs}/aN^{1/2} = f_{bb}(X, Z), \quad X = N^{1/2}\sigma, \quad Z = N^{1/2}\tau \qquad (8)$$

At large enough grafting density, one can describe the bottle-brush as a compact filling of a cylinder of radius, R_{cs}, with thermal blobs: the density inside the cylinder does *not* depend on σ, and to achieve this, the chains are still somewhat stretched away from the cylinder axis, although one is under poor solvent conditions!

We can estimate the cylinder cross-sectional radius, R_{cs}, simply by the condition that in a disk of volume $R_{cs}^2\pi/\sigma$ there is one chain with N monomers grafted, and the density in such a disk, $\rho = N\sigma/(R_{cs}^2\pi)$, must be equal to the density in the blobs, eq 7. This condition yields

$$R_{cs}^2/(a^2 N) \propto \xi_T \sigma \propto X/Z \qquad (9)$$

To estimate the boundaries of the region in the XZ plane, where eq 9 holds, we observe that eq 9 can only hold if ξ_T exceeds the thickness σ^{-1} of the considered disk, that is

$$\xi_T \sigma = 1 \Rightarrow X = Z \qquad (10)$$

where again prefactors of order unity were ignored. At this lower "phase boundary" of the regime of the cylindrical brush, the cross-sectional radius is then equal to the ideal radius of a single chain, $R_{cs}^2 = a^2N$.

The other boundary of this regime of slightly stretched brushes is reached when the radius predicted by eq 9 becomes of the same order as the radius at the theta point, eq 4, that is, $R_{cs}^2/a^2N \propto X^{2/3} \propto X/Z$, and hence the boundary where a smooth crossover from $R_{cs} \propto N^{1/2}$ to $R_{cs} \propto N^{2/3}$ occurs is given by

$$Z \propto X^{1/3}, \quad \sigma \propto N\tau^3 \tag{11}$$

The most interesting regime occurs for $Z > X$, however, where a homogeneous filling of a cylinder with thermal blobs is not favorable because the blob diameter is smaller than the distance between grafting sites along the cylinder axis. It turns out that then the structure of the brush along the cylinder axis is inhomogeneous. Of course, for very small grafting density, each grafted mushroom collapses independently; in eq 8, the scaling argument $X \approx 0$, and we simply recover a backbone with independently collapsed mushrooms, which are globules as described by eq 6. A naive treatment would suggest that the regime of these isolated globules of eq 6 extends up to the point where neighboring independent globules start to "touch" and hence interact, that is, $R_{glob}\sigma = 1$ or $X^3 = Z$. However, it turns out that this boundary can only be considered to be a kind of stability limit of the "phase" of independent globules, but actually, another state takes over at much smaller grafting density than that predicted by this simplistic argument. As pointed out by Sheiko et al.,[29] the state of independent globules is unfavorable because of its high cost of surface free energy, and a more favorable state is already reached for

$$Z = X^{-3} \tag{12}$$

where several neighboring mushrooms stretch to form jointly a cluster of extension L along the backbone and radius $R_{cluster}$

$$L \propto N^{1/2}(\tau/\sigma)^{1/4}, \quad R_{cluster} \propto N^{1/2}(\sigma/\tau)^{1/4} \tag{13}$$

and the number of chains per cluster is predicted to be $n_{cluster} = N^{1/2}\tau^{1/4}\sigma^{3/4} = (X^3Z)^{1/4}$; that is, it varies from $n_{cluster} = o(1)$ near $Z = X^{-3}$ to $n_{cluster} = X$ near $X = Z$, where also $L \approx R_{cluster} \approx aN^{1/2}$; whereas, in general, the aspect ratio $L/R_{cluster} \propto (\tau/\sigma)^{1/2} = (Z/X)^{1/2}$ leads to very elongated cluster shapes. At the border of the cluster regime (where eq 12 holds), L is of the order of σ^{-1}, the distance between the grafting sites.

Figure 2 collects these findings in a "phase diagram", where eqs 10−12 are shown as thick lines, and configuration snapshots of the model studied here are included in the respective regions, as already presented in a short communication.[31]

We now discuss the extension of these considerations from the one-component case to the two-component case. Whereas, on a mean-field level, the chain collapse of single chains occurs (in the limit $N \to \infty$) when the Flory−Huggins parameter χ exceeds a critical value ($\chi_{crit} = 1/2$)[58,69,70] for two types of side chains grafted to the backbone, we need to distinguish not only two different chain lengths (N_A,N_B) but also three different Flory−Huggins parameters, χ_{AA}, χ_{BB}, and χ_{AB}. Whereas in a dense molten polymer blend, it is only the combination $\chi_{mix} = \chi_{AB} - (\chi_{AA} + \chi_{BB})/2$ that controls phase separation between species A and B in this blend,[58,69,70] the problem of phase separation between two polymers in bulk solution in a common solvent is much more complex.[70] Here we shall not address the most general case of a binary bottle-brush polymer, but restrict attention only to the most symmetric model

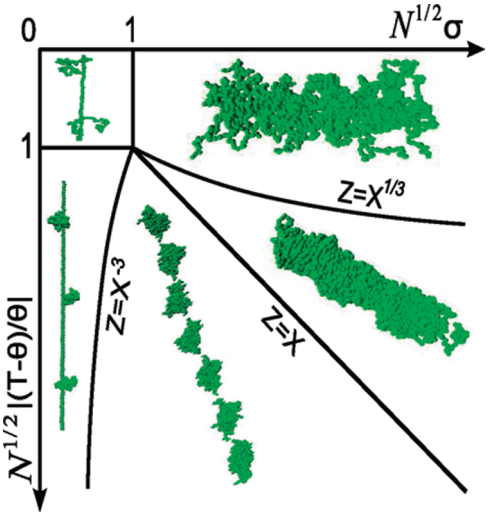

Figure 2. Schematic phase diagram of a (single-component) bottle-brush polymer with a rigid backbone, under poor solvent conditions, in the plane of scaling variables $X = N^{1/2}\sigma$ and $Z = N^{1/2}(1 - T/\Theta)$. The lines $X = 1$ and $Z = 1$ in the upper left corner enclose the regime where the grafted side chains are essentially independent "polymer mushrooms", obeying essentially Gaussian chain statistics because of the proximity of the theta point. When the line $X = 1$ is crossed, a gradual crossover to a bottle-brush under theta conditions occurs, as described by eqs 3 and 4. When the line $Z = 1$ is crossed, a gradual crossover from the Gaussian mushrooms $R \propto N^{1/2}$ to collapsed independent globules occurs, as described by eqs 5 and 6. Near the line $Z = X^{1/3}$, the crossover from the "theta brush" to the collapsed cylindrical brush occurs, which is described by eq 9, whereas at the line $X = Z$, the crossover to clusters (with properties described in eq 13) occurs, whereas the line $Z = X^{-3}$ describes the crossover to the collapsed globules. Simulation snapshots (using the model of Section III) illustrate the various structures.

$$N_A = N_B = N, \quad \chi_{AA} = \chi_{BB} = \chi \tag{14}$$

Whereas in the general case for two polymers A, B in a particular solvent the theta temperatures Θ_A, Θ_B will differ, eq 14 implies $\Theta_A = \Theta_B = \Theta$ and hence greatly simplifies the situation. According to the Flory−Huggins mean-field approximation for such a symmetric blend in a common solvent, unmixing occurs for[70]

$$\chi_{mix} > \chi_{crit} = 2/[N\phi] \tag{15}$$

where ϕ is the fraction of lattice sites occupied by the two types of monomers (while a fraction $1 - \phi$ of the sites of the considered lattice model then is taken by the solvent molecules). Because $\phi \propto \rho$, cf. eq 7, we conclude

$$\chi_{crit} \propto 1/[N(1 - T/\Theta)] \tag{16}$$

for the regime of the collapsed brush in Figure 2.

The problem of phase separation of symmetric binary bottle-brush polymers has been treated before by Stepanyan et al.[32] using arguments based on the self-consistent field theory. It was also proposed that for brushes at the theta point one has[29]

$$\chi_{crit} \propto N^{-2/3} \tag{17}$$

Using eq 11 for the crossover from the collapsed bottle-brush to the theta brush, $\tau = 1 - T/\Theta \propto (\sigma/N)^{1/3}$, a smooth crossover occurs from $\chi_{crit} \propto [N(1 - T/\Theta)]^{-1}$ to $[N^{2/3}\sigma^{1/3}]^{-1}$, consistent with eq 17.

Whereas Stepanyan et al.[32] as well as subsequent simulation work[33] did address only dense cylindrical bottle-brushes and assumed that the phase separation that occurs is of the Janus cylinder-type, Hsu et al.[26] pointed out that for choices where $\chi_{mix} \gg \chi$, the formation of A−B interfaces, which must occur when the Janus cylinder-type of microphase separation is chosen, is energetically very unfavorable, and rather a structure with a "double-cylinder" cross-section was proposed.[26] In the present work, we want to consider even additional structures, whose occurrence is plausible in view of the phase diagram for the single-component bottle-brush, Figure 2: given the fact that in a broad range of grafting densities for $T < \Theta$ a pearl-necklace-type structure occurs, with two types (A, B) of chains, microphase separation within individual pearls also becomes conceivable as well as the formation of an alternating sequence of A-rich pearls and B-rich pearls along the backbone of the bottle-brush. The latter situation would be reminiscent of microphase separation of a block copolymer melt confined into a cylinder,[71] whereas the case of microphase separation inside of individual pearls might give rise to the formation of a Janus particle-like structure (if an A−B interface in the cluster is present) or of dumbbell-like clusters, where the A-chains and B-chains are separated in the two parts of the dumbbell.

Noting that the volume of a cluster is of order $R_{cluster}^2 L \propto N^{3/2}(\sigma/\tau)^{1/4}$ and comprises $Nn_{cluster} \propto N^{3/2}\tau^{1/4}\sigma^{3/4}$ monomers, eq 13 implies that the monomer density in a "pearl" (or "cluster") is

$$\rho_{cluster} \propto Nn_{cluster}/R_{cluster}^2 L \propto (\tau\sigma)^{1/2} \tag{18}$$

which has to be compared with the density $\rho \propto \tau$ in the dense cylindrical brush, which occurs if $\sigma > \tau$ (cf. eq 10). Therefore, we see that in the regime of interest $\rho_{cluster} < \rho$ but for $\sigma \propto \tau$, a smooth crossover from $\rho_{cluster}$ to ρ occurs, as expected. The condition for microphase separation in a cluster hence becomes, generalizing eq 16, for $\tau > N^{-1/2}$

$$\chi_{mix} > \chi_{crit} \propto 1/\{N[(1 - T/\Theta)\sigma]^{1/2}\}, \quad N^{-2/3}\tau^{-1/3} < \sigma < \tau \tag{19}$$

As we shall see in Section IV, phase separation in single clusters actually is easily observable. Of course, also, these "transitions" in binary bottle-brush polymers should not be treated as sharp phase transitions: in dense cylindrical brushes, rounding of the transition is caused by the quasi-1D nature of the system, as was already discussed by Hsu et al.[26,34] For phase separation of single pearls or clusters, the rounding of the transitions should even be more pronounced because of the finite number of chains in these clusters, and neighboring clusters can undergo phase separation independent of each other.

III. Model and Simulation Methods

As in the above theoretical considerations, the model treated via molecular dynamics simulations considers only a bottle-brush with a strictly rigid backbone, where hence side chains are simply grafted at an immobile straight line in the z direction (where also periodic boundary conditions are applied, so effects due to the chain ends of the backbone polymer are completely outside of consideration).

Clearly, this choice is a stringent approximation and not strictly realizable in experiments, but in studies of bottle-brush polymers under good solvent conditions,[72] it was shown that already for moderately short side chain length a considerable backbone stiffening is indirectly induced; therefore, quantities such as radial monomer density profiles for bottle-brushes with rigid and with flexible backbones are almost indistinguishable. Simulation studies of de Jong and ten Brinke[33] indicate that also under theta conditions there is still a great similarity between the rigid and flexible backbone case. Under poor solvent conditions, however, pearl-necklace structures for certain choices of parameters may collapse into rather dense arrangements.[33,73] Such phenomena hence are out of consideration here. We also note that semiflexible chains in bad solvent show not only globules but also toroidal and disk-like structures,[74,75] and we expect that similar structures should occur for bottle-brush polymers with flexible backbones in poor solvents, too. However, a thorough study of this situation must be left to a later investigation.

The side chains are modeled by the standard bead−spring model,[36,40,64] where all beads interact with a truncated and shifted Lennard-Jones potential

$$U_{LJ}(r) = \begin{cases} 4\epsilon_{LJ}[(\sigma_{LJ}/r)^{12} - (\sigma_{LJ}/r)^{6}] + C, & r \le r_c \\ 0, & r > r_c \end{cases} \tag{20}$$

where $r_c = 2.5\sigma_{LJ}$, and the constant C is defined such that $U_{LJ}(r = r_c)$ is continuous at the cutoff. Henceforth units are chosen such that $\epsilon_{LJ} = 1$, $\sigma_{LJ} = 1$, $k_B = 1$, and the mass m of the beads also is taken to be unity. When we consider two types (A,B) of side chains, we still use $\sigma_{LJ}^{AA} = \sigma_{LJ}^{AB} = \sigma_{LJ}^{BB} = 1$, $\epsilon_{LJ}^{AA} = \epsilon_{LJ}^{BB} = 1$ but $\epsilon_{LJ}^{AB} = 1/2$ or (alternatively) $\epsilon_{LJ}^{AB} = 3/4$ to create an unmixing tendency. When one considers a binary system of monomers at density $\rho = 1$, such a Lennard-Jones mixture is a standard system for the study of phase separation, which occurs below a critical temperature, T_c, close to $T = 1.5$.[76] For the polymer bottle-brush, the average densities are much smaller, but because the critical temperature $T_c \propto \chi_{crit}^{-1}$, scales proportional to the side chain length (eqs 16 and 19), we do expect to be able to detect microphase separation with our model.

The connectivity of the beads along a side chain is maintained by the "finitely extensible nonlinear elastic" (FENE) potential

$$U_{FENE}(r) = -\frac{1}{2} k r_0^2 \ln[1 - (r/r_0)^2], \quad 0 < r \le r_0 \tag{21}$$

where the standard choice of parameters ($r_0 = 1.5$, $k = 30$) was adopted and $U_{FENE}(r > r_0) = \infty$ constrains the bond lengths.

In the one-component case, four choices of side chain length were studied, namely, $N = 20$, 35, 50, and 100. Although these chains perhaps are not long enough to verify some of the scaling predictions discussed in Section II, we note that bottle-brushes studied in experimental work have side chain lengths in a range quite comparable to that of our work.[1−12] The number of side chains was typically $M = 50$; therefore, the backbone length, L_b, was simply given by $L_b = M/\sigma$. As noted above, periodic boundary conditions in the z direction along the rigid backbone were used; also, in the x,y directions, periodic boundary conditions were used, but the considered linear dimensions of the simulation box were chosen to be large enough so that never any interaction of the bottle-brush with its periodic images did occur. Note that we did not include any explicit solvent particles; solvent-mediated interactions and solvent quality are only indirectly simulated by varying the temperature of the system.

For the model defined by eqs 20 and 21, unfortunately, the theta temperature is known only rather roughly,[36] namely, $\Theta \approx 3.0$. Being interested in $T \le \Theta$, we have attempted to study the temperature range $1.5 \le T \le 3.0$. Note, however, that equilibration of collapsed chains is rather difficult, as will be discussed below. In our simulations, temperature is controlled by the

Langevin thermostat, as done in a previous work.[31,36,40,64] The equation of motion for the coordinates $\{\vec{r}_i(t)\}$ of the beads

$$m\frac{d^2\vec{r}_i}{dt^2} = -\nabla U_i - m\gamma\frac{d\vec{r}}{dt} + \vec{\Gamma}_i(t) \quad (22)$$

is numerically integrated using the GROMACS package.[77] In eq 22, t denotes the time, U_i is the total potential acting on the ith bead, γ is the friction coefficient, and $\vec{\Gamma}_i(t)$ is the random force. As is well-known, γ and $\vec{\Gamma}_i(t)$ are related by the usual fluctuation−dissipation relation

$$\langle\vec{\Gamma}_i(t)\cdot\vec{\Gamma}_j(t')\rangle = 6k_BT\gamma\delta_{ij}\delta(t-t') \quad (23)$$

Following previous work,[36,40,64] the friction coefficient was chosen as $\gamma = 0.5$. Equation 22 was integrated with the leapfrog algorithm[78] using an integration time step of $\Delta t = 0.006\tau$, where the MD time unit $\tau = (m\sigma_{LJ}^2/\epsilon_{LJ})^{1/2} = 1$ in our units.

First, the system was equilibrated at the temperature $T = 3.0$ using simulations extending over a time range of $30 \times 10^6\tau$. To gather statistics, for $\sigma = 0.0355$, 0.38, and 1.51, we used 500 statistically independent configurations at this high temperature as initial configurations for "slow cooling" runs, where the temperature was lowered in steps of 0.1, and the system was run at each temperature for a time of $5 \times 10^5\tau$. The final configuration of each (higher) temperature was used as starting configuration for the next (lower) temperature. In this way, one can generate at low temperatures and intermediate values of the grafting densities configurations of clusters that are statistically independent of each other. In the microphase separated state, it is completely impossible to run a single system long enough that the chains sample the different configurations according to which they can be assigned to different clusters; if some chains have joined at $T = 1.5$ to form a cluster, then transitions where a chain leaves a cluster to join a neighboring cluster are prohibitively difficult. Therefore, standard MD runs at these low temperatures would not sample phase space adequately. This problem is avoided by carrying out these 500 independent slow cooling runs, and we have checked (by variation of the cooling speed and of the number of runs) that this high statistical effort was just enough to obtain meaningful results. Therefore, it is not possible to study longer chains in this way.

For all temperatures, T, and all grafting densities, σ, that were studied, we also carried out runs where the temperature was changed in one step from $T = 3.0$ to the desired temperature, where after an equilibration period of again $30 \times 10^6\tau$, sampling of the properties of the system every 1000 τ was done. Whereas with this traditional method along the lines of previous work[36,40,64] we obtained reliable results for $T \geq 2.0$, the resulting properties did not show any significant dependence on the "different history of sample preparation", a detailed analysis of the data show that for $T < 2.0$ this "fast cooling" method is less reliable, as expected. In particular, for $T = 1.5$ (and for both intermediate and high grafting densities, where nontrivial density correlations in the z direction along the backbone occur), we found that for the fast cooling procedure these long-range density correlations are systematically underestimated. This finding is not surprising because in such inhomogeneous systems, free energy barriers are expected, which slow down the relaxation, and thus the intrinsic relaxation times exceed the time scale of the MD simulation.

For the binary bottle-brushes, a less complete parameter variation has been performed, but all data generated were based on the slow cooling method. In fact, one must expect that concentration fluctuations and density fluctuations in this system are strongly coupled, and additional free energy barriers to relax the local concentration fluctuations (which may require that a chain center of mass moves along the chain backbone a distance of the order of the gyration radius of the chain, through a dense environment, and respecting all grafting constraints of the chains) must be expected.

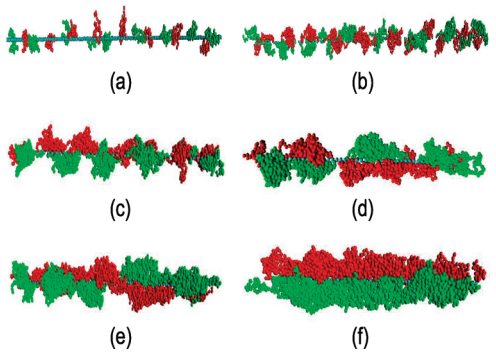

Figure 3. Snapshot pictures for binary bottle-brushes at $T = 1.5$, $N_A = N_B = N = 35$, and various grafting densities: σ = (a) 0.12, (b) 0.38, (c) 0.57, (d) 0.76), (e) 1.14, and (f) 1.51. Note that chains are grafted regularly at distances σ^{-1} along the backbone, and A-chains and B chains (distinguished by different color or greytone) alternate. Units in z direction are smaller than in radial directions by factors (a) 1.6, (b) 1.3, (c) 1, (d) 1, (e) 1, and (f) 1.

To give the reader a feeling for the difficulties that need to be overcome, we present some snapshot pictures for binary bottle brush polymers (Figure 3). At $T = 1.5$, only for $\sigma = 0.12$ most of the chains are still in the regime of independently collapsed mushrooms, and for $\sigma = 1.51$, a more-or-less homogeneous structure along the z axis is present, and microphase separation clearly can be recognized (a detailed analysis shows, however, that there is hardly any A−B interface present, so the structure is not a Janus cylinder). For intermediate grafting densities (such as $\sigma = 0.38$, 0.57, 0.76, and 1.14) one can see that both microphase separation and cluster formation occur. Whereas qualitative observations of similar character were already reported in the literature,[33] the distinctive feature of the present work is an extensive analysis of long-range axial correlations of both the density and composition variations in the system, on the basis of our well-equilibrated data.

IV. Results

Following our discussion in Section. II, we start by presenting the radial density profiles $\rho(r)$ of the bottle-brush polymers in typical cases (Figures 4 and 5) and discuss also the dependence of the cross-sectional radius, R_{cs}, defined as (note the normalization $2\pi\sigma^{-1}\int_0^\infty \rho(r)r\,dr = N$)

$$R_{cs} = (2\pi/N\sigma)\int_0^\infty \rho(r)r^2\,dr \quad (24)$$

on grafting density, chain length, and temperature (Figure 6). In the density profile $\rho(r)$ one can see rather strong oscillations for small r, reminiscent of the "layering" of the density when one considers the packing of fluid particles near hard walls. One would expect, in the spirit of Figure 1, that for somewhat larger values of r, where these density oscillations have decayed, one finds a region of constant density (cf. eq 7), whereas in the outermost "shell of blobs", the density $\rho(r)$ decreases to zero gradually, resembling the density profile across an interface between coexisting polymer-rich and pure solvent phases in a polymer solution under poor solvent conditions, where phase separation has occurred. However, we find that this interfacial profile is rather broad, at least for the relatively small values of the side chain length studied here, and thus the picture of a cylinder

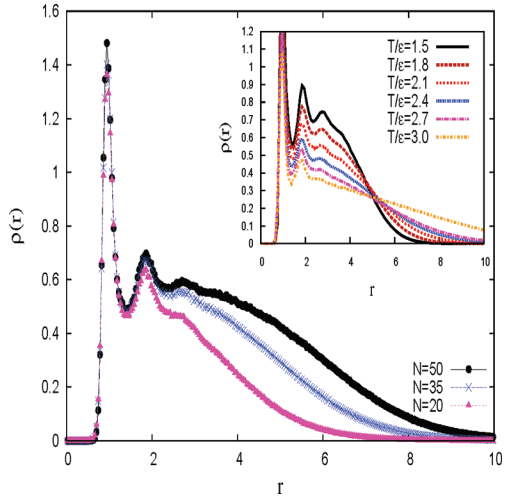

Figure 4. Typical result for $\rho(r)$ versus r for a bottle-brush polymer with only one type of side chains at a high grafting density ($\sigma = 1.51$) at a temperature $T/\epsilon = 2.1$ (moderately poor solvent quality) for the chain lengths $N = 20$, 35, and 50, as indicated. Inset shows the variation of the density profile for $N = 35$ with temperature.

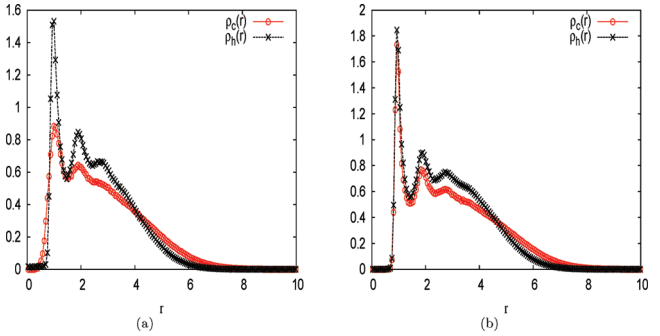

Figure 5. Density profiles $\rho_h(r)$ versus r (for one-component bottle-brushes) and $\rho_c(r)$ versus r (for two-component bottle-brushes) for $T/\epsilon = 1.5$, $N = 35$, and two grafting densities: $\sigma =$ (a) 1.14 and (b) 1.51.

and its interior is an oversimplification, at least for the conditions accessible in our study, we recall, however, that these conditions also are typical for experimental studies.[1−12,14−16]

The inset of Figure 4 shows the temperature variation of $\rho(r)$: the change of the profile is completely gradual; as expected, there is no singular behavior visible in our data when in the diagram of states (Figure 2) the crossover line $Z = X^{1/3}$ is passed.

Whereas Figure 4 considers only the largest grafting density ($\sigma = 1.51$) that we have studied, Figure 5 presents data for our lowest temperature ($T/\epsilon = 1.5$) for two grafting densities, and we compare here the density profiles of the one-component homopolymer brushes, $\rho_h(r)$, to the density profiles $\rho_c(r)$ of the two-component copolymer brushes, where alternatingly side chains of type A and B are grafted. Whereas for $\sigma = 0.38$ (not shown here), the differences between $\rho_h(r)$ and $\rho_c(r)$ are still minor; with increasing σ, one notes that $\rho_c(r) < \rho_h(r)$ for small r but $\rho_c(r) > \rho_h(r)$ for larger r. This difference is already a clear indication that the simple picture of a "Janus cylinder" is not an accurate description: It has already been pointed out by Hsu et al.[26] that the Janus cylinder[8] forms only if the interfacial free energy γ_{AB} between unmixed A-rich and B-rich phases is sufficiently low in comparison with the surface free energy γ of the cylinder (Figure 7). Remember[58,70] that γ_{AB} is controlled by the quantity χ_{mix}, which is, in our model, proportional to $(\epsilon_{LJ}^{AA} + \epsilon_{LJ}^{BB})/2 - \epsilon_{LJ}^{AB} = 1/2$, wheras $\gamma_{AA} = \gamma_{BB} = \gamma$ is proportional to $\epsilon_{LJ}^{AA} = \epsilon_{LJ}^{BB} = 1$ for the chosen energy parameters. Depending on

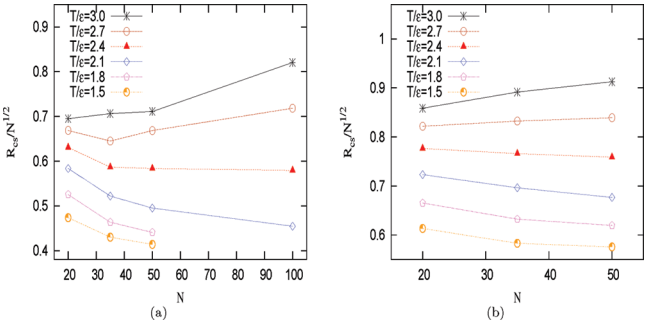

Figure 6. Normalized cross-sectional radius $R_{cs}/N^{1/2}$ plotted versus chain length, N, and various temperatures for the grafting densities $\sigma =$ (a) 0.38 and (b) $\sigma = 1.51$.

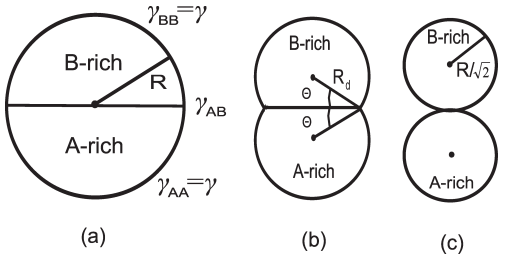

Figure 7. Schematic cross sections through collapsed binary bottle-brushes at high grafting density under very poor solvent conditions, where sharp interfaces between A-rich and B-rich regions and the solvent occur. If the interfacial tension γ_{AB} is low enough, then the (local) cross-section is a "Janus cylinder", that is half of the cylinder is taken by the A-rich phase and half by the B-rich phase, with a planar interface in between (case a). If γ_{AB} in comparison with $\gamma_{AA} = \gamma_{BB} = \gamma$ exceeds a critical value, then a dumbbell-shaped cross-section appears (b), whereas at still larger γ_A, a "double cylinder"-type cross-section appears (c). In the latter case, the radius of each cylinder simply is $R/\sqrt{2}$ if the cross-sectional radius of the Janus cylinder is R.

chain length and the distance from the theta conditions, the ratio γ_{AB}/γ can in general be varied over a wide range, however,[70] and hence also structures with dumbbell-like cross-section (Figure 7b) or "double cylinder" cross-section (Figure 7c) become possible. For the dumbbell-type cross-section, the total surface free energy cost is, per unit length along the cylinder axis

$$F_{surf} = \gamma 2R_d(\pi + \Theta) + \gamma_{AB} 2R_d \cos\Theta \qquad (25)$$

with $R_d = R, \Theta = 0$ in the "Janus cylinder" case and $R_d = R/\sqrt{2}$, $\Theta = \pi/2$ in the double-cylinder case, whereas in between we have

$$R_d = R/\sqrt{1 - 2\Theta/\pi + \pi^{-1}\sin 2\Theta} \qquad (26)$$

Minimizing F_{surf} with respect to Θ, taking the constraint eq 26 into account, it is possible to find Θ and R as a function of γ_{AB}/γ and use then the resulting shape of the contour in Figure 7 together with the assumption that the density $\rho(r) = \rho =$ const inside of the contour and $\rho(r) = 0$ in the outside region to compute R_{cs} from eq 24. However, because we have seen from Figure 4 that all of our data are far from the region where the approximation of a sharp outer surface of the cylinder is reasonable, we have not worked out this approximation further.

To check whether Figure 7a (Janus cylinder), Figure 7b (Janus dumbbell), or Figure 7c (double cylinder) occurs for our specific choice of interactions, we compute the number of contacts among AA, AB, and BB pairs of monomers. Whereas for the lattice model of Hsu et al.,[26,34] because of the discreteness of the lattice, the counting of nearest neighbor contacts is well-defined and straightforward; for an off-lattice model in the continuum, there

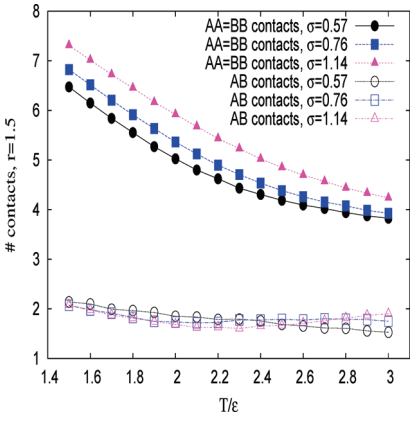

Figure 8. Number of contacts for AA and BB pairs (full symbols) and for AB pairs (open symbols, data have been multiplied by a factor of 10 for better visibility) plotted versus T/ϵ and three grafting densities, as indicated. As a neighborhood criterion, it was used that the distance between two monomers must not exceed $r_c = 1.5\sigma_{LJ}$ for the pair to be counted as a "contact".

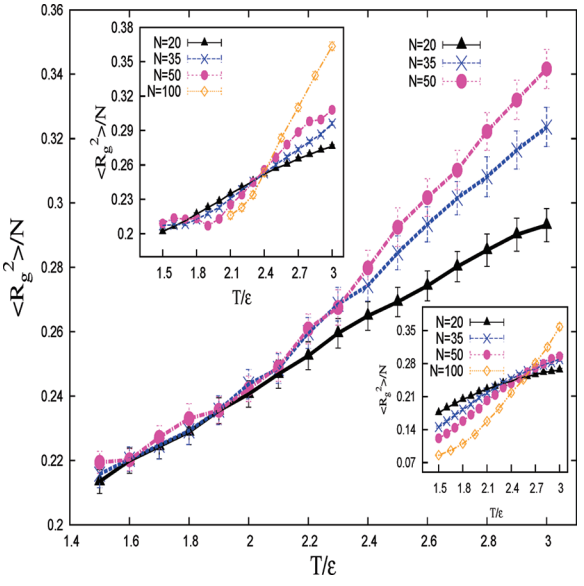

Figure 9. Mean square radius of gyration $\langle R_g^2 \rangle$ of the side chain normalized with their chain length N plotted versus temperature T/ϵ for $\sigma = 1.51$ and three chain lengths. Left inset shows analoguous data for $\sigma = 0.38$, whereas the right inset shows data in the mushroom regime ($\sigma = 0.0355$).

is inevitably some arbitrary choice to be made, at which distance one stops counting particles as still being "bound together" by the attractive interactions. We have followed the standard convention that two monomers form a contact if their distance does not exceed $1.5\sigma_{LJ}$.[79] To check how sensitive the data are to this particular choice of cutoff, we also tested a second choice ($1.2\sigma_{LJ}$). Apart from the fact that for this shorter range the contact numbers are systematically smaller, the trend with the temperature is very similar, and hence we feel that our qualitative conclusions are not affected by this choice.

Figure 8 shows these contact numbers for $N = 35$ as a function of temperature for three grafting densities. Note that by the symmetry of our model, the number of AA contacts and of BB contacts should be identical, and within our statistical errors (which do not exceed the size of the symbols, in Figure 8), this symmetry is nicely verified. We see that when T/ϵ is reduced from the theta region ($T/\epsilon \approx 3.0$)) to $T/\epsilon = 1.5$, the number of these contacts between the same type of monomers increases from about 4 to about 7. In a dense fluid, still larger effective coordination numbers are expected, but this is not seen here because there are many monomers in the outer region of the bottle-brush, where the density gradually decreases (Figure 4) and hence also the number of neighbors within the interaction range decreases.

Note that the number of unlike contacts has been multiplied by 10 so that it becomes more visible on the scale of the graph. This number of unlike contacts stays almost the same at low T as in the theta region, near 0.2, and also shows only a weak dependence on grafting density. Of course, if a Janus cylinder forms, then only monomers along the A−B interface plane can yield AB contacts, and so this contact number must be much smaller than for AA and BB contacts. But we would expect a strong increase with decreasing temperature, similarly as for the AA and BB contacts. On the basis of these data, the most likely structure model in our case is the Janus dumbbell. If a double cylinder would form, then we would expect that the number of unlike neighbors decreases with decreasing temperature (as in fact was seen in the lattice model of Hsu et al.[26,34]), and this is not seen either.

Apart from the cross-sectional radius of the bottle-brush as a whole, it is also of great interest to consider the linear dimensions of individual chains in the bottle-brush, of course. Figure 9 shows the temperature dependence of $\langle R_g^2 \rangle/N$ for several chain lengths and grafting densities in the one-component case. First of all, we draw attention to the right inset, where $\langle R^2 \rangle/N$ is plotted versus temperature at very small grafting density, so that one can observe the collapse of individual mushrooms. In this case, one expects that $\langle R_g^2 \rangle/N \propto N^{2\nu-1} \approx N^{0.118}$ for $T > \Theta$, $\langle R_g^2 \rangle/N \propto$ const (independent of N) for $T = \Theta$, and $\langle R_g^2 \rangle/N \propto N^{-1/3}$ for $T < \Theta$. Therefore, plotting $\langle R_g^2 \rangle/N$ versus T for various N, one should be able to locate the theta temperature from a common intersection point of these curves.[80] However, the data show a considerable scatter of the intersection points of the various $\langle R_g^2 \rangle/N$ versus T curves, in the region $2.4 < T/\epsilon < 2.7$, which is well below the estimate $\Theta \approx 3.0$[36] obtained for single chains of this model. Of course, the scaling considerations of Section II imply that in principle one should keep the scaling variable $X = N^{1/2}\sigma$ fixed at a very small value when one varies N and T to study the left side of the phase diagram (Figure 2). However, for the chosen chain lengths ($N \leq 100$), the grafting density $\sigma = 0.0355$ is small enough such that interactions between neighboring mushrooms along the backbone are still negligible. Therefore, we maintain that for the chosen chain lengths, even isolated mushrooms in the regime $T/\epsilon > 2.7$ are still somewhat swollen. Of course, we cannot exclude that much longer chains exhibit in this regime a tendency toward collapse; such a slow approach to the asymptotic behavior was seen in some models.[81]

However, for larger grafting densities such as $\sigma = 0.38$, where chains do not yet form a cylindrical structure uniformly along the z axis, we find a rather well-defined intersection point at $T/\epsilon \approx 2.4$ (left inset). Conversely, we can conclude that for this grafting density, chain stretching (rather than swelling) sets in for $T/\epsilon > 2.4$. For the high grafting density ($\sigma = 1.51$), this regime of chain stretching even starts at $T/\epsilon \approx 2.1$ already (Figure 9). The fact that with increasing σ the regime of chain stretching extends to lower temperatures is in (qualitative) accord with the scaling considerations of Section II (cf. eq 11). For the large grafting density $\sigma = 1.51$, a detailed structural analysis clearly reveals that the bottle-brush forms a cylindrical structure with essentially uniform density along the z direction. The regime where we have $\langle R_g^2 \rangle/N$ independent of N for an extended regime of temperatures (namely, $1.5 < T/\epsilon < 2.1$ in Figure 9) corresponds to the regime of the dense cylindrical brush (from $Z = X$ to $Z = X^{1/3}$) in Figure 2.

It also is of interest to study individual components of the chain radii, in particular, when one considers intermediate values of the grafting density, where the pearl-necklace structure occurs.

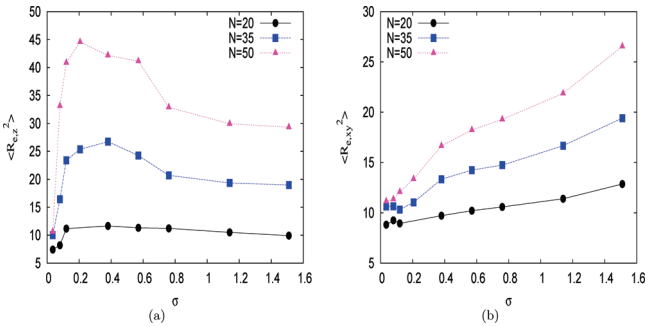

Figure 10. Mean square end-to-end distance components (a) parallel ($\langle R^2_{e,z}\rangle$) and (b) perpendicular ($\langle R^2_{e,xy}\rangle$) to the cylinder axis at $T/\epsilon = 1.5$ plotted versus σ, for three different chain lengths, as indicated.

Figure 10 shows the mean square end-to-end distance $\langle R^2_{e,z}\rangle$ and $\langle R^2_{e,xy}\rangle$ of single chains at $T/\epsilon = 1.5$, resolved in components along the cylinder axis and perpendicular to it. One can clearly see that for $\sigma \approx 0.1$, the axial component $\langle R^2_{e,z}\rangle$ rises dramatically to large values, whereas the perpendicular component stays small and rises with increasing σ later and rather slowly. In this regime, $\langle R^2_{e,z}\rangle$ decreases again; less stretching in axial direction is needed to form the clusters with neighboring chains along the backbone. These observations confirm the theoretical predictions of Sheiko et al.,[29] eq 13, at least qualitatively.

This behavior does carry over with little modification to the binary bottle brushes. Figure 11 shows the temperature dependence of the end-to-end mean square radii components. Whereas $\langle R^2_{e,xy}\rangle$ is monotonically decreasing with decreasing temperature, one finds that $\langle R^2_{e,z}\rangle$ exhibits a shallow minimum, and for T/ϵ less

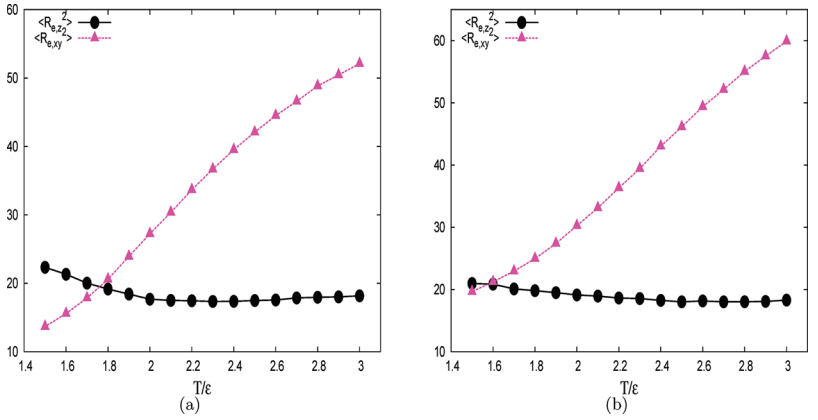

Figure 11. Mean square end-to-end distance components parallel ($\langle R^2_{e,z}\rangle$) and perpendicular ($\langle R^2_{e,xy}\rangle$) to the cylinder axis plotted versus temperature at various grafting densities: (a) $\sigma = 0.38$, and (b) $\sigma = 1.14$. All data refer to $N = 35$.

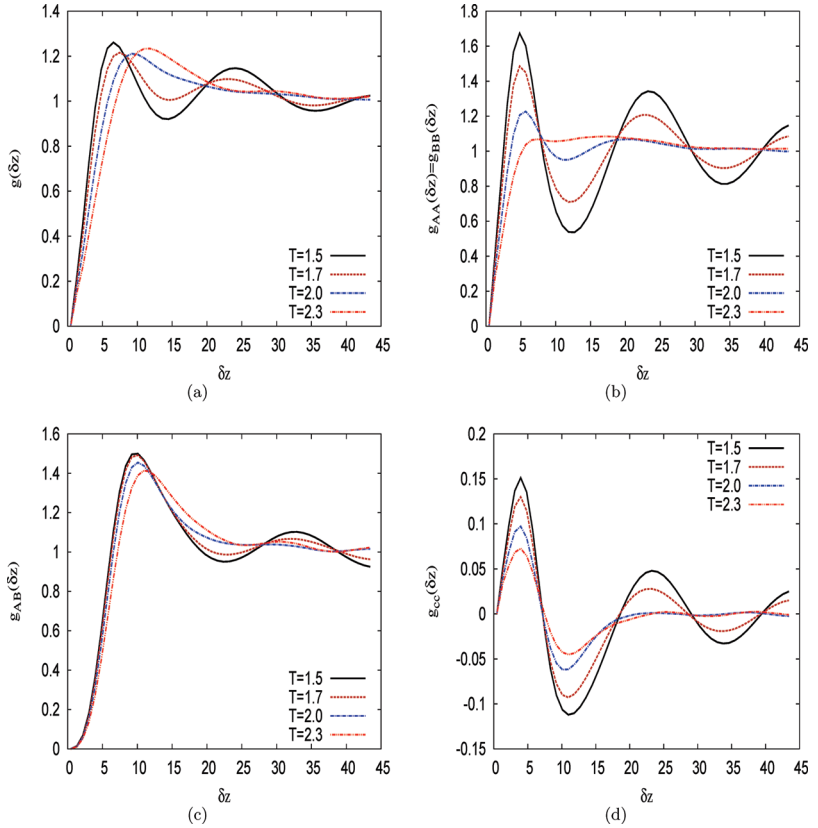

Figure 12. (a) Density correlations $g(\delta z)$, (b) partial correlations $g_{AA}(\delta z)$, (c) $g_{AB}(\delta z)$, and (d) concentration correlation $g_{cc}(\delta z)$ plotted versus δz for the case $\sigma = 0.57$, $N = 50$. Please note that $g_{BB}(\delta z) = g_{AA}(\delta z)$ because of the symmetry of the model and hence is not shown. Different curves show various temperatures, as is indicated.

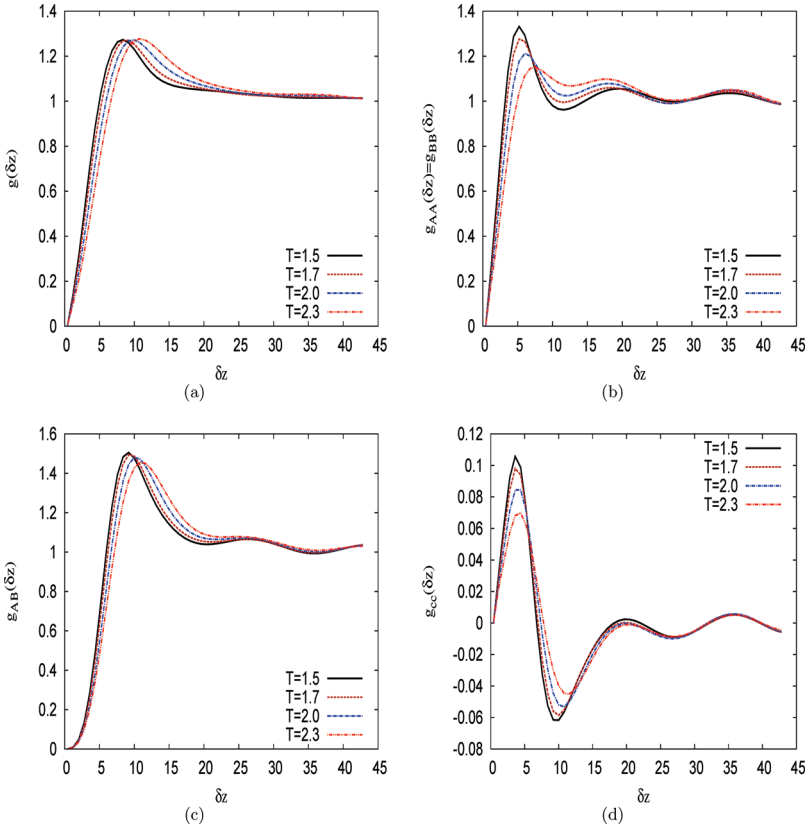

Figure 13. Same as Figure 12, but for the case $\sigma = 1.14$, $N = 35$. In this case, a backbone of twice the length as in Figure 12 was used (100 grafted chains).

than about $T/\epsilon = 2.0$, this component increases again. Whereas in the dense collapsed cylindrical state the linear dimensions $\langle R^2_{e,xy}\rangle$ and $\langle R^2_{e,z}\rangle$ again are about the same, for small σ such as $\sigma = 0.206$, again $\langle R^2_{e,z}\rangle$ is distinctly larger, indicating that the axial stretching is once more operative.

We now turn to fluctuations of collective properties such as the densities $\rho_A(z)$, $\rho_B(z)$, and $\rho(z) = \rho_A(z) + \rho_B(z)$ and ask, in particular, how are the fluctuations of these quantities correlated in the z direction along the backbone of the bottle-brush? Following standard practice in the bulk, the following correlation functions are defined

$$g_{AA}(\delta z) = \langle \rho_A(z)\rho_A(z+\delta z)\rangle / \rho_A^2 \tag{27}$$

$$g_{AB}(\delta z) = \langle \rho_A(z)\rho_B(z+\delta z)\rangle / \rho_A\rho_B \tag{28}$$

and

$$g_{BB}(\delta z) = \langle \rho_B(z)\rho_B(z+\delta z)\rangle / \rho_B^2 \tag{29}$$

Note that the averages $\langle ...\rangle$ in eqs 27−29 are meant to include an average over the coordinate z along the backbone as well: apart from the fact that the grafting sites of the A-chains and B-chains alternate regularly at distances $\Delta z = \sigma^{-1}$ along the z axis, the system is translationally invariant in the z direction. Therefore, we have $\rho_A \equiv \langle \rho_A(z)\rangle = \langle \rho_A(z+\delta z)\rangle$ and $\rho_B = \langle \rho_B(z)\rangle = \langle \rho_B(z+\delta z)\rangle$, and hence the correlation functions in eqs 27−29 are defined such that, in the disordered phase

$$g_{AA}(\delta z \to \infty) \to 1, \quad g_{AB}(\delta z \to \infty) \to 1, \quad g_{BB}(\delta z \to \infty) \to 1 \tag{30}$$

Because we are interested in the correlations of the total density $\rho(z) = \rho_A(z) + \rho_B(z)$ and of the relative concentration $c(z) = [\rho_A(z) - \rho_B(z)]/\rho$, we consider also the following linear combinations of the above correlations[76,82]

$$g(\delta z) = x_A^2 g_{AA}(\delta z) + 2x_A x_B g_{AB}(\delta z) + x_B^2 g_{BB}(\delta z) \tag{31}$$

$$g_{cc}(\delta z) = x_A^2 x_B^2 [g_{AA}(\delta z) + g_{BB}(\delta z) - 2g_{AB}(\delta z)] \tag{32}$$

where $x_A = \rho_A/(\rho_A + \rho_B)$ and $x_B = \rho_B/(\rho_A + \rho_B)$. In our case, $x_A = x_B = 1/2$, of course.

Figures 12 and 13 show typical examples of these functions. It is interesting to observe that these functions do show pronounced oscillations, but the maxima and minima occur at somewhat shifted positions. Furthermore, these extrema sometimes have a pronounced dependence on temperature. For example, in the case $\sigma = 0.57$, $N = 50$, one finds that at higher temperatures, $g(\delta z)$ has a single maximum (near $\delta z = 11$ at $T = 2.3$). When the temperature is lowered, this maximum gradually shifts toward smaller δz, for example, $\delta z = 6.5$ for $T = 1.5$, a pronounced minimum (near $\delta z = 14$), and a second maximum (near $\delta z = 23$) develops as well. In $g_{AA}(\delta z)$, however, the first maximum develops at $\delta z = 6$ and shifts down to $\delta z = 5$ as the temperature is lowered. In $g_{cc}(\delta z)$, the first peak occurs for $\delta z = 4$, and a minimum is present for $\delta z = 11$; here the features get more pronounced as the temperature gets lowered, but the locations of these extrema do not shift.

Interestingly, the second peak of all of these quantities occurs at roughly the same spot; of course, $g_{AB}(\delta z)$ behaves quite differently. (A maximum develops roughly in the region where g_{cc} has its minimum because A-monomers and B-monomers try to avoid each other.) A similar correlation can also be seen for the case $N = 50, \sigma = 0.76$, the main difference being that the peaks of $g(\delta z)$, $g_{AA}(\delta z)$ have shifted to large values of δz, and even at low temperature, a second maximum can no longer be clearly identified. For $g_{AB}(\delta z)$, it is particularly clear that there exists

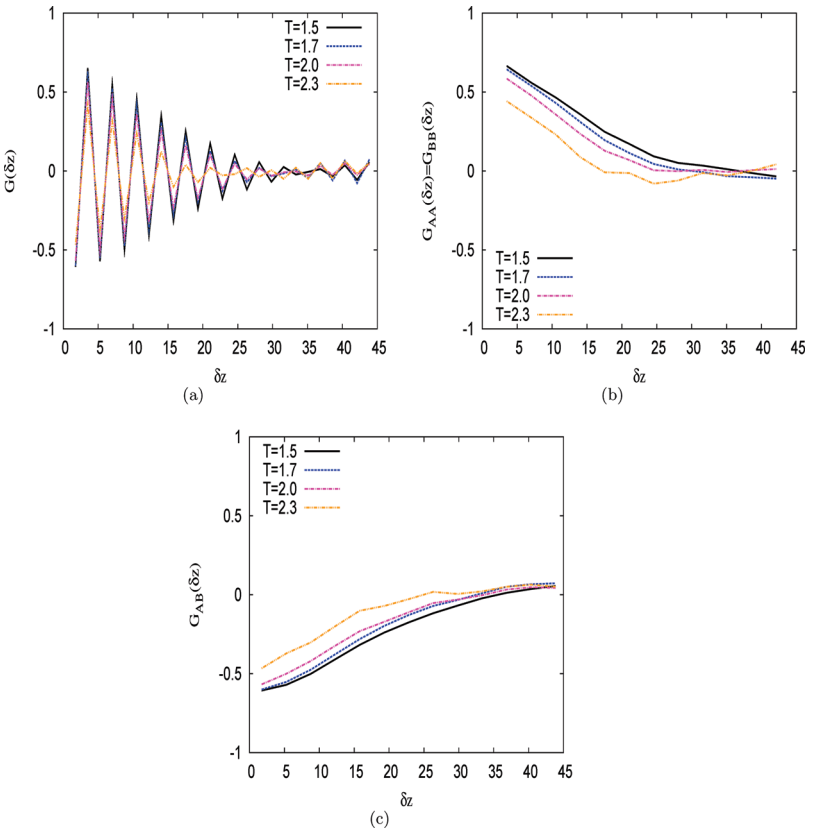

Figure 14. Correlation function (a) $G(\delta z)$, (b) $G_{AA}(\delta z)$, and (c) $G_{AB}(\delta z)$ describing the projection of the unit vectors from the grafting sites of the chains to their center of mass into the xy plane onto each other as a function of the distance δz along the backbone, for the case $N = 50$, $\sigma = 0.57$, and the same temperatures as in Figure 12.

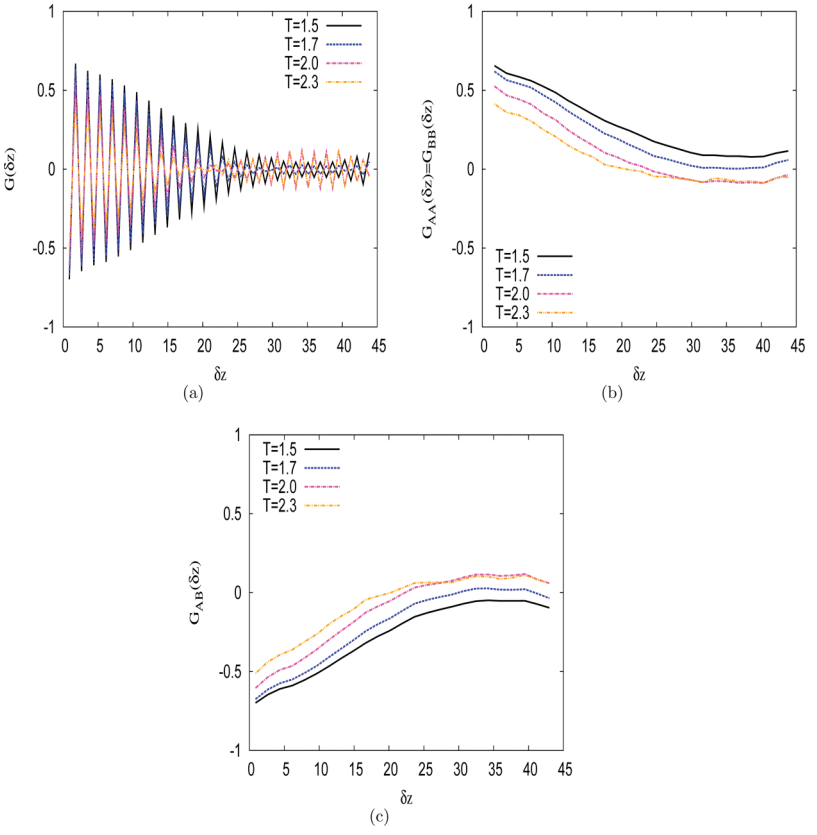

Figure 15. Same as Figure 14 but for the case $\sigma = 1.14$, $N = 35$. In this case, a backbone of twice the length as in Figure 14 was used (100 grafted chains).

only a single maximum. This tendency continues for $\sigma = 1.14$ (Figure 13): also, $g(\delta z)$ now has a single maximum only, which for $T = 1.5$ occurs near $\delta z \approx 8$, whereas $g_{cc}(\delta z)$ has a maximum at $\delta z \approx 4$ (and a second, weaker, maximum near $\delta z \approx 20$).

These data indicate that the interplay between density and concentration fluctuations in these mixed bottle-brushes leads to rather complex structural rearrangements. Therefore, we have also looked at the Fourier transform of these correlation functions. We found that for the case $\sigma = 1.14$, $N = 35$ a rather sharp peak due to block copolymer-like mesophase formation occurs at $q \approx 0.3$. (This is seen in both $S_{AA}(q)$, $S_{BB}(q)$, $S_{cc}(q)$ and $S_{AB}(q)$ (which is negative), but not in the total structure factor $S(q)$). For $\sigma = 0.57$ and 0.76, the structure factors turn out to be rather irregular, indicating insufficient statistical averaging over the irregular pearl-necklace-type structures (Figure 3) that prevail in this regime.

Finally, Figures 14 and 15 study the correlation of an order parameter (already introduced by Hsu et al.[26,34]) to monitor the extent over which the Janus cylinder-type order (or Janus dumbbell-type order) is correlated along the backbone. We consider for each chain the vector pointing from the grafting site to the center of mass of respective side chain. Projecting this vector into the xy plane and defining a unit vector $\vec{S}_i^{\alpha}$ along the projection (α = A or B), we define the correlation functions

$$G(\delta z) = \langle \vec{S}_i^{\alpha} \cdot \vec{S}_j^{\beta} \rangle,$$

$$G_{AA}(\delta z) = \langle \vec{S}_i^{\alpha} \cdot \vec{S}_j^{\alpha} \rangle \quad (\alpha = A, B, \beta = A, B)$$

and

$$G_{AB}(\delta z) = \langle \vec{S}_i^{\alpha} \cdot \vec{S}_j^{\beta} \rangle, \beta \neq \alpha \tag{33}$$

Note that in $G(\delta z)$ all chains are correlated (irrespective of whether they are of type A or B), whereas in $G_{AB}(\delta z)$, one considers the correlation of unlike chains only. Indeed, Figures 14 and 15 demonstrate that rather long-range Janus-type correlations do develop in our model. (Of course a true long-range order for quasi-1D systems is not expected.[26,34])

V. Conclusions

In the present investigation, simulations of a bead−spring model of flexible polymers grafted onto a rigid backbone and variable solvent conditions (from the region of the theta temperatures to the region of moderately poor solvents) were considered. The main interest of this work has been the microphase separation between two types (A, B) of equally long side chains, but also additional results for the case of homopolymer bottle-brushes for otherwise identical parameters of grafting density, σ, and side chain length, N, are given, and a (qualitative) comparison with pertinent theoretical predictions (which we have summarized in Section II) has been made.

In the homopolymer case, we have confirmed the diagram of states (Figure 1) proposed by Sheiko et al.[29] and presented evidence of the axial stretching of the chains (Figure 10a) in the intermediate regime of grafting densities under poor solvent conditions, where a few neighboring chains cluster together to form pearls of a strongly elongated shape, cf. eq 13 and subsequent discussion. This formation of elongated pearls shows up in the nonmonotonic variation of $\langle R_{e,z}^2 \rangle$ with σ. The steep uprise of $\langle R_{e,z}^2 \rangle$ near $\sigma \approx 0.05$ and the decrease near $\sigma \approx 0.7$ can be taken as estimates for the boundaries of this elongated pearl-necklace structure in Figure 2, namely, the boundaries denoted by $Z = X^{-3}$ and $Z = X$, respectively. We recall that because of the quasi-1D character of our system, for any $N < \infty$, these transition lines in Figure 2 are not sharply defined phase boundaries in the sense of thermodynamic phase diagrams but rather indicate qualitatively the location of gradual crossovers. These crossovers become presumably the more rapid the larger the chain length; however, for our choices of N (=20, 35, 50), it would be premature to attempt an extrapolation to the limit $N \to \infty$. We note, however, that our range of N is the same range that also is practically realizable in experiments.

The main interest of our study was then to clarify how this picture gets modified when one considers symmetric binary systems with $N_A = N_B = N$, and energy parameters $\epsilon_{AA} = \epsilon_{BB} = \epsilon$, $\epsilon_{AB} = \epsilon/2$ that give rise to a microphase separation between A and B, as qualitatively already demonstrated in the snapshot pictures. At small grafting densities, A and B chains along the backbone collapse independently of each other (Figure 3), whereas for larger σ, one has again a clustering of neighboring chains into elongated pearls, in which now microphase separation between A and B has taken place. At high grafting density, the snapshot (Figure 3f) at first sight looks like a Janus cylinder structure, but a more detailed analysis shows that the structure of the local cross sections is not of Janus cylinder-type (Figure 7a) but rather of Janus dumbbell-type (Figure 7b). Evidence of this assertion comes from the fact that the radial density profiles (Figure 5) in the binary case extend to somewhat larger distances than in the homopolymer case and from an analysis of the temperature dependence of the various binary contact numbers (Figure 8).

Finally, we have also analyzed various correlations along the axial direction (Figures 12−15) to test to what extent precursors of Janus cylinder (or Janus dumbbell-type, respectively) long-range order in the z direction occurs. In our rather densely collapsed bottle-brushes, this ordering is found to extend over many side chains along the backbone and hence is of truly mesoscopic character. However, we expect that the microphase separation will be strongly affected when the condition of perfect rigidity of the backbone is somewhat relaxed. We intend to study the case of flexible backbones in future work, and this will also allow us to make closer contact to various experiments.

Acknowledgment. P.E.T. is grateful to the Max Planck Institute for Polymer Research (Mainz) for support via a Max Planck Fellowship. We acknowledge computing time on the Softcomp and Juropa clusters of the Jülich Supercomputing Centre (JSC and NIC).

References and Notes

(1) Tsukahara, Y.; Mizuno, K.; Segawa, A.; Yamashita, Y. *Macromolecules* **1989**, *22*, 1546.
(2) Wintermantel, M.; Schmidt, M.; Tsukahara, Y.; Kajiwara, K.; Kohjiya, S. *Macromol. Rapid Commun.* **1994**, *15*, 279.
(3) Wintermatnel, M.; Gerle, M.; Fischer, K.; Schmidt, M.; Wataoka, I.; Urakawa, H.; Kajiwara, K.; Tsukahara, Y. *Macromolecules* **1996**, *29*, 978.
(4) Beers, K. L; Gaynor, S. G.; Matyaszewski, K.; Sheiko, S. S.; Möller, M. *Macromolecules* **1998**, *31*, 9413.
(5) Lecommandoux, S.; Chilecot, F.; Borsali, R.; Schappacher, M.; Deffieux, A.; Brûlet, A.; Cotton, J. P. *Macromolecules* **2002**, *35*, 8878.
(6) Stephan, T.; Muth, S.; Schmidt, M. *Macromolecules* **2002**, *35*, 9857.
(7) Li, C.; Gunari, N.; Fischer, K.; Janshoff, A.; Schmidt, M. *Angew. Chem., Int. Ed.* **2004**, *43*, 1101.
(8) Liu, Y.; Abetz, V.; Müller, A. H. E. *Macromolecules* **2003**, *36*, 7894.
(9) Zhang, M.; Müller, A. H. E. *J. Polym. Sci., Part A: Polym. Chem.* **2005**, *43*, 3461.
(10) Rathgeber, S.; Pakula, T.; Matyjaszewski, K.; Beers, K. L *J. Chem. Phys.* **2005**, *122*, 124904.

(11) Zhang, B.; Gröhn, F.; Pedersen, J. S.; Fischer, K.; Schmidt, M. *Macromolecules* **2006**, *39*, 8440.
(12) Feuz, L.; Strunz, P.; Geue, T.; Textor, M.; Borisov, O. *Eur. Phys. J E.* **2007**, *23*, 237.
(13) Subbotin, A. V.; Semenov, A. N. *Polym. Sci., Ser. A* **2007**, *49*, 1328.
(14) Sheiko, S. S.; Sumerlin, B. S.; Matyjaszewski, K. *Prog. Polym. Sci.* **2008**, *33*, 759.
(15) Lee, H. I.; Matyjaszewski, R.; Yu-Su, S.; Sheiko, S. S. *Macromolecules* **2008**, *41*, 6073.
(16) Knaapilo, M.; Stepanyan, R.; Torkkeli, M.; Garamus, V. M.; Galbrecht, F.; Nehls, B. S.; Preis, E.; Scherf, U.; Monkman, A. P. *Phys. Rev. E* **2008**, *77*, 051809.
(17) Klein, J. *Science* **2009**, *323*, 47.
(18) Hsu, H.-P; Paul, W.; Rathgeber, S.; Binder, K. *Macromolecules* **2010**, *43*, 1592.
(19) Shiokawa, K.; Itoh, K.; Nemoto, M. *J. Chem. Phys.* **1999**, *111*, 8165.
(20) Subbotin, A.; Saariaho, M.; Ikkala, O.; ten Brinke, G. *Macromolecules* **2000**, *33*, 3447.
(21) Chang, R.; Kwak, Y.; Gebremichael, Y. J. *Mol. Biol.* **2009**, *391*, 648.
(22) Elli, S.; Ganazzoli, F.; Timoshenko, E. G.; Kuznetsov, Y. A.; Connolly, R. *J. Chem. Phys.* **2004**, *120*, 6257.
(23) Connolly, R.; Bellesia, G.; Timoshenko, E. G.; Kuzentsov, Y. A.; Elli, S.; Ganazzoli, F. *Macromolecules* **2005**, *38*, 5288.
(24) Yethiraj, A. *J. Chem. Phys.* **2006**, *125*, 204901.
(25) Rathgeber, S.; Pakula, T.; Wilk, A.; Matyajazewski, K.; Lee, H.-I.; Beers, K. L. *Polymer* **2006**, *47*, 7318.
(26) Hsu, H.-P.; Paul, W.; Binder, K. *Macromol. Theory Simul.* **2007**, *16*, 660.
(27) Hsu, H.-P.; Paul, W.; Binder, K. *J. Chem. Phys.* **2008**, *129*, 204904.
(28) Hsu, H.-P.; Paul, W.; Binder, K., preprint **2009**.
(29) Sheiko, S. S.; Borisov, O. V.; Prokhorova, S. A.; Möller, M. *Eur. Phys. J. E* **2004**, *13*, 125.
(30) Khalatur, P. G.; Shirvanyanz, D. G.; Staravoitova, N. Y.; Khokhlov, A. R. *Macromol. Theory Simul.* **2000**, *9*, 141.
(31) Theodorakis, P. E.; Paul, W.; Binder, K. *Europhys. Lett.* **2009**, *88*, 63002.
(32) Stepanyan, R.; Subbotin, A.; ten Brinke, G. *Macromolecules* **2002**, *35*, 5640.
(33) de Jong, J.; ten Brinke, G. *Macromol. Theory Simul.* **2004**, *13*, 318.
(34) Hsu, H.-P.; Paul, W.; Binder, K. *Europhys. Lett.* **2006**, *76*, 526.
(35) Lai, P.-Y.; Binder, K. *J. Chem. Phys.* **1992**, *97*, 586.
(36) Grest, G. S.; Murat, M. *Macromolecules* **1993**, *26*, 3108.
(37) Yeung, C.; Balazs, A. C; Jasnow, D. *Macromolecules* **1993**, *26*, 1914.
(38) Tang, H.; Szleifer, I. *Europhys. Lett.* **1994**, *28*, 19.
(39) Carignano, M. A.; Szleifer, I. *J. Chem. Phys.* **1994**, *100*, 3210.
(40) Grest, G. S.; Murat, M. In *Monte Carlo and Molecular Dynamics Simulations in Polymer Science*; Binder, K., Ed.; Oxford University Press: New York, 1995; p 476.
(41) Szleifer, I.; Carignano, M. A. *Adv. Chem. Phys.* **1996**, *94*, 165.
(42) Marko, J. F.; Witten, T. *Macromolecules* **1992**, *25*, 296.
(43) Lai, P. Y. *J. Chem. Phys.* **1994**, *100*, 3351.
(44) Brown, G.; Chakrabarti, A.; Marko, J. F. *Europhys. Lett.* **1994**, *25*, 239.
(45) Müller, M. *Phys. Rev. E* **2002**, *65*, 030802.
(46) Wenning, L.; Müller, M.; Binder, K. *Europhys. Lett.* **2005**, *71*, 639.
(47) Borisov, O. V.; Zhulina, E. B.; Birshtein, T. M. *Polym. Sci. U.S.S.R., Ser. A* **1998**, *30*, 772.
(48) Zhulina, E. B.; Borisov, O. V.; Pryamitsyn, V. A.; Birshtein, T. M. *Macromolecules* **1991**, *24*, 140.
(49) Halperin, A.; Tirell, M.; Lodge, T. P. *Adv. Polym. Sci.* **1992**, *100*, 31.
(50) Amoskov, V. M.; Birshtein, T. M. *Macromol. Theory Simul.* **2009**, *18*, 453.
(51) Imry, Y.; Ma, S. K. *Phys. Rev. Lett.* **1975**, *35*, 1399.
(52) Nattermann, T. In *Spin Glasses and Random Fields*, Young., A. P. (Ed.) World Scientific, Singapore, 1998, p 277.
(53) Binder, K.; Kob, W. *Glassy Materials and Disordered Solids: An Introduction to Their Statistical Mechanics*; World Scientific: Singapore, 2005.
(54) Leibler, L. *Macromolecules* **1980**, *13*, 1602.
(55) Hamley, I. W. *The Physics of Block Copolymers*; Oxford University Press: New York, 1998.
(56) Landau, L. D., Lifshitz, E. M. *Statistical Physics*; Pergamon Press, Oxford, U.K., 1958.
(57) Baxter, R. J. *Exactly Solvent Models in Statistical Mechanics*; Academic Press: New York, 1982.
(58) de Gennes, P. G. *Scaling Concepts in Polymer Physics*; Cornell University Press, Ithaca, NY, 1979.
(59) Birshtein, T. M.; Zhulina, E. B. *Polymer* **1984**, *25*, 1453.
(60) Witten, T. A.; Pincus, P. A. *Macromolecules* **1986**, *19*, 2509.
(61) Birshtein, T. M.; Borisov, O. V.; Zhulina, E. B.; Khokhlov, A. R.; Yurosowa, T. A. *Polym. Sci. U.S.S.R.* **1987**, *29*, 1293.
(62) Ligoure, C.; Leibler, L. *Macromolecules* **1990**, *23*, 5044.
(63) Ball, R. C.; Marko, J. F.; Milner, S. T.; Witten, T. A. *Macromolecules* **1991**, *24*, 693.
(64) Murat, M.; Grest, G. S. *Macromolecules* **1991**, *24*, 704.
(65) Rouault, Y.; Borisov, O. V. *Macromolecules* **1996**, *29*, 2605.
(66) Saariahko, M.; Ikkala, O.; Szleifer, I.; Erukhimovich, I.; ten Brinke, G. *J. Chem. Phys.* **1997**, *107*, 3267.
(67) Le Guillou, J. C.; Zinn-Justin, J. *J. Phys. Rev. B* **1980**, *21*, 3976.
(68) de Gennes, P. G. *Macromolecules* **1980**, *13*, 1069.
(69) Flory, P. J. *Principles of Polymer Chemistry*; Cornell University Press: Ithaca, NY, 1953.
(70) Binder, K. *Adv. Polym. Sci.* **1994**, *112*, 181.
(71) Erukhimovich, I.; et al., in preparation.
(72) Hsu, H.-P.; Binder, K.; Paul, W. *Phys. Rev. Lett.* **2009**, *103*, 198301.
(73) Vasilevskaya, V. V.; Klochkov, A. A.; Khalatur, P. G.; Khokhlov, A. R.; ten Brinke, G. *Macromol. Theory Simul.* **2001**, *10*, 389.
(74) Ivanov, V. A.; Paul, W.; Binder, K. *J. Chem. Phys.* **1998**, *109*, 5659.
(75) Stukan, M. R.; Ivanov, A. V.; Grosberg, A. Yu.; Paul, W.; Binder, K. *J. Chem. Phys.* **2003**, *118*, 3392.
(76) Das, S. K.; Horbach, J.; Binder, K. *J. Chem. Phys.* **2003**, *119*, 1547.
(77) http://www.gromacs.org; For original papers on this code, see: (a) Berendsen, H. J. C.; van der Spoel, D.; van Drunen, R. *Comput. Phys. Commun.* **1995**, *91*, 43; (b) Lindahl, E.; Hess, B.; van der Spoel, D. *J. Mol. Mod.* **2001**, *7*, 306. (c) van der Spoel, D.; Lindahl, E.; Hess, B.; Groenhof, G.; Mark, A. E.; Berendsen, H. J. C. *J. Comput. Chem.* **2005**, *26*, 1701. (d) Hess, B.; Kutzner, C.; van der Spoel, D.; Lindahl, E. *J. Chem. Theory Comput.* **2008**, *4*, 435.
(78) Van Gunsteren, W. F.; Berendsen, H. J. C. *Mol. Simul.* **1988**, *1*, 173.
(79) Stillinger, F. H. *J. Chem. Phys.* **1963**, *38*, 1486.
(80) *Monte Carlo and Molecular Dynamics Simulations in Polymer Science*; Binder, K., Ed.; Oxford University Press: New York, 1995.
(81) Graessley, W. W.; Hayward, R. C,; Grest, G. S. *Macromolecules* **1999**, *32*, 3510.
(82) Bhatia, A. B.; Thornton, D. E. *Phys. Rev. B* **1970**, *2*, 3004.